

Motion Direction Detection from Segmentation by LIAC, and Tracking by Centroid Trajectory Calculation

Antonio Fernández-Caballero

Escuela Politécnica Superior de Albacete, Departamento de Informática
Universidad de Castilla-La Mancha, 02071 – Albacete, Spain

Abstract. Motion information can form the basis of predictions about time-to-impact and the trajectories of objects moving through a scene. Firstly, a model that incorporates accumulative computation and lateral interaction is presented. By means of the lateral interaction in accumulative computation (LIAC) of each element with its neighbours, the model is able to segment moving objects present in an indefinite sequence of images. In a further step, moving objects are tracked using a centroid-based trajectory calculation.

1 Motion Direction Detection

Motion plays an important role in our visual understanding of the surrounding environment [1]. Visual motion can aid in the detection of shape [2], provide information as to the relative depth of moving objects [3], and give clues about the material properties of moving objects, such as the rigidity and transparency [4]. Motion information can also form the basis of predictions about time-to-impact and the trajectories of objects moving through a scene [5]. This paper introduces a novel method for motion direction detection based on segmentation by lateral interaction in accumulative computation (LIAC) and tracking by centroid trajectory calculation.

1.1 Segmentation from LIAC

The aim of segmentation step is firstly to determine in what grey level stripe a given element (x,y) falls. Let $GLS(x,y,t)$ be the grey level stripe of image pixel (x,y) at time t and n the total number of grey level stripes.

$$GLS(x,y,t) = \frac{256}{n}, \quad n \in [1, 256] \quad (1)$$

Lateral interaction in accumulative computation is capable of modelling the motion on the image, starting from the pixel grey level stripe and the element state or permanence value. There are as many permanence values for a given element as grey level stripes. At each time instant t , the permanence value is obtained in two steps. (1) A charge or discharge due to the motion detection, that's to say, due to a change in the grey level stripe, and, (2) a re-charge due to the lateral interaction on the partially

charged elements that are directly or indirectly connected to maximally charged elements. The charge or discharge behaviour of the permanence memory is explained next. (a) All permanence values not associated to grey level stripe k are completely discharged down to value v_{dis} . (b) If the pixel associated to the element is enclosed in grey level stripe k , we are in front of two different possibilities. (b.1) If the pixel was not enclosed in grey level stripe k in time $t-1$, permanence memory is completely charged up to the maximum value v_{sat} , or, (b.2) if the pixel was previously enclosed in grey level stripe k in time $t-1$, permanence memory is applied a decrement of value v_{dm} (discharge value due to motion detection), down to a minimum of v_{dis} .

$$PM(k, x, y, t) = \begin{cases} v_{dis}, & \text{if } GLS(x, y, t) \neq k \\ v_{sat}, & \text{if } GLS(x, y, t) = 1 \text{ and } GLS(x, y, t-1) \neq k \\ \max(PM(k, x, y, t-1) - v_{dm}, v_{dis}), & \text{if } GLS(x, y, t) = k \text{ and } GLS(x, y, t-1) = k \end{cases} \quad (2)$$

If the element is charged to the maximum, it informs its neighbours through the channels prepared for this use. This is the way a re-charge of the permanence value due to lateral interaction by a value v_{rv} (charge value due to vicinity) can now be performed. This functionality is biologic and can be seen as an absolute refractory period adaptive mechanism. Obviously, the permanence memory cannot be charged over the maximum value v_{sat} . Note that this is the way the system is able to maintain our attention on an element, just because it is connected to a maximally charged element up to l pixels away, and the false background motion is eliminated.

$$PM(k, x, y, t) = \min(PM(k, x, y, t) + \varepsilon \cdot v_{rv}, v_{sat}), \quad (3)$$

$$\text{where } \varepsilon = \begin{cases} 1, & \text{if } \exists (1 \leq i \leq l) \wedge \forall (1 \leq j \leq i) \\ & (PM(k, x, y+i, t) = v_{sat} \cap PM(k, x, y+j, t) > v_{dis}) \cup \\ & (PM(k, x+i, y, t) = v_{sat} \cap PM(k, x+j, y, t) > v_{dis}) \cup \\ & (PM(k, x, y-i, t) = v_{sat} \cap PM(k, x, y-j, t) > v_{dis}) \cup \\ & (PM(k, x-i, y, t) = v_{sat} \cap PM(k, x-j, y, t) > v_{dis}) \\ 0, & \text{otherwise} \end{cases} \quad (4)$$

1.2 Centroid Trajectory Calculation

The last step consists in obtaining the trajectory of the objects by spatio-temporally calculating the centroid (X_{obj}, Y_{obj}) of the maximally charged pixels of the moving objects. Fig. 1 graphically shows the calculation of the centroid of an object.

Therefore the size is defined starting from the longitude of two right lines (or cords) determined by four well-known pixels of the surface of the object [6]. The pixels referenced this way are (x_1, y_1) , (x_2, y_2) , (x_3, y_3) and (x_4, y_4) , such that:

$$\forall (x, y) \in S(i, j, t), \quad x_1 < x, \quad x_2 > x, \quad y_3 < y, \quad y_4 > y \quad (5)$$

In other words, the four pixels are:

- (x_1, y_1) : pixel most at the left of the object in the image
- (x_2, y_2) : pixel most at the right of the object in the image
- (x_3, y_3) : upper most pixel of the object in the image
- (x_4, y_4) : lower most pixel of the object in the image

The two cords denominated maximum line segments of the object, won't unite the

pixels (x_1, y_1) and (x_2, y_2) , (x_3, y_3) and (x_4, y_4) to each other, but rather their projections $(X_1, 0)$ and $(X_2, 0)$, $(0, Y_3)$ and $(0, Y_4)$, respectively, as you can appreciate in Fig. 1.

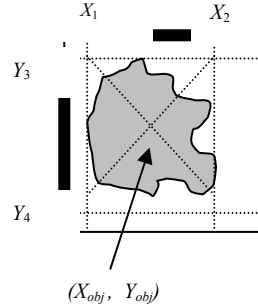


Fig. 1. Centroid of an object

Now, the object's location will be determined by a unique characteristic pixel (X_{obj}, Y_{obj}) , that is to say, the intersection of the two segments $(X_1, Y_3)(X_2, Y_4)$ and $(X_2, Y_3)(X_1, Y_4)$. This centroid pixel will be denominated representative pixel of the object.

Once the maximum line segments and the representative pixel of an object have been obtained in a sequence of images, it should be rather simple to detect a lot of motion cases [7],[8]. Anyway, considering the following possibilities: no motion (N), translation in X or Y-axis (T), dilation, or translation in Z-axis (D), and, rotation (R), we may only obtain, by combining them, the following possibilities:

N	no motion	TDR	translation + dilation + rotation
T	pure translation	D	pure dilation
TD	translation plus dilation	DR	dilation plus rotation
TR	translation plus rotation	R	pure rotation

It is considered that the previous states appear in most cases (Fig. 2). Fig. 2 shows the different possibilities when no change is detected in the representative pixels coordinates enclosed in brackets. When there is a significant change in the co-ordinates of the representative pixel, a T has been added enclosed in parenthesis. In this graph:

- (1) Comparison between the horizontal maximum line segments of previous $(k-1)$ and current (k) image

$$\begin{cases} \text{Larger,} & \text{if } (X_2 - X_1)_k - (X_2 - X_1)_{k-1} > l \\ \text{Equal,} & \text{if } (X_2 - X_1)_k - (X_2 - X_1)_{k-1} = l \\ \text{Smaller,} & \text{if } (X_2 - X_1)_k - (X_2 - X_1)_{k-1} < l \end{cases} \quad (6)$$

where l is the maximum permitted difference.

- (2) Comparison between the vertical maximum line segments of previous $(k-1)$ and current (k) image

$$\begin{cases} \text{Larger,} & \text{if } (Y_4 - Y_3)_k - (Y_4 - Y_3)_{k-1} > l \\ \text{Equal,} & \text{if } (Y_4 - Y_3)_k - (Y_4 - Y_3)_{k-1} = l \\ \text{Smaller,} & \text{if } (Y_4 - Y_3)_k - (Y_4 - Y_3)_{k-1} < l \end{cases} \quad (7)$$

where l is the maximum permitted difference.

- (3) Similitude degree between the scale change of the maximum segments of images at $k-1$ and k

$$\left\{ \begin{array}{l} \text{Similar,} \\ \text{Different,} \end{array} \right. \text{ if } 1 - \alpha \leq \frac{\frac{(X_2 - X_1)_k}{(Y_4 - Y_3)_k}}{\frac{(X_2 - X_1)_{k-1}}{(Y_4 - Y_3)_{k-1}}} \leq 1 + \alpha \quad (8)$$

where α is the permitted fluctuation in the similitude function.

- (4) Result state if the representative pixel of the object has not changed substantially; a non substantial change is obtained by means of the following algorithm
- $$(X_{objk} - X_{objk-1} \leq d) \cap (Y_{objk} - Y_{objk-1} \leq d) \quad (9)$$

where d is the maximum permitted displacement.

- (5) Result state if the representative pixel of the object has changed substantially.

Of course, the possibility to offer some erroneous results with an unknown error rate is assumed, especially in front of some rotation examples. Nevertheless, if the number of images in a sequence is great enough, this error rate should be very little.

(1)	(2)	(3)	(4)	(5)
		Similar	[D]	(TD)
	Larger	Different	[DR]	(TDR)
Larger	Equal		[R]	(TR)
	Smaller		[R]	(TR)
	Larger		[R]	(TR)
Equal	Equal		[N]	(T)
	Smaller		[R]	(TR)
	Larger		[R]	(TR)
Smaller	Equal		[R]	(TR)
	Smaller	Similar	[D]	(TD)
		Different	[DR]	(TDR)

Fig. 2. Motion states graph

2 Some Illustrative Examples

The algorithms exposed previously have been applied to multitude of synthetic sequences as shown in Fig. 3.

In example 1, a pure translation in one of the axis, in particular in the y -axis, is shown. The algorithms work perfectly in this easy case (outputs is always D), even in presence of the gleaned form of the treated object. Pure translations in the three axes x , y , z have been all tested with this same and other synthetic objects. They have offered the same good results in their behaviour. Evidently, it was expected that this simple case had to work that well.

The second example is representative of more complex translation movements. Here there are simultaneous translations in several axes. All possible translation combinations have been tested, obtaining for all the analysed objects an excellent behaviour of the algorithms. This concrete example offers the translation motion of an

irregular form in the three axes in a simultaneous way. That is the reason why the correct result TD appears in all twenty steps of the approached synthetic sequence.

As it was easy to foresee, the problems would begin when incorporating rotational movements. Example 3 is a sample of it. Indeed, we are in front of the case of a cube approaching on z -axis and rotating simultaneously. Notice that the algorithm does not throw the desired result DR, but a simple D, in the simulations. The explanation has to be looked for in the shape of the object. Indeed, the algorithm works so much better for the case of rotations the more irregular the shape of the analysed object's motion is. Unfortunately, the horizontal and vertical segments always have the same value for this figure.

Example 4 analyses a similar motion to the one of example 3. Here, nevertheless, we are in front of an irregular shape. So it was waited to get a better behaviour of the algorithms exposed in this work. And, indeed, good results are obtained from the analysis of image 9 on of the sequence. The explanation of why the first images do not throw the desired result is in the value chosen for the allowed fluctuation ($\alpha=0,2$) in the similitude function of the motion evaluation graph. A smaller value allows improving the previous results.

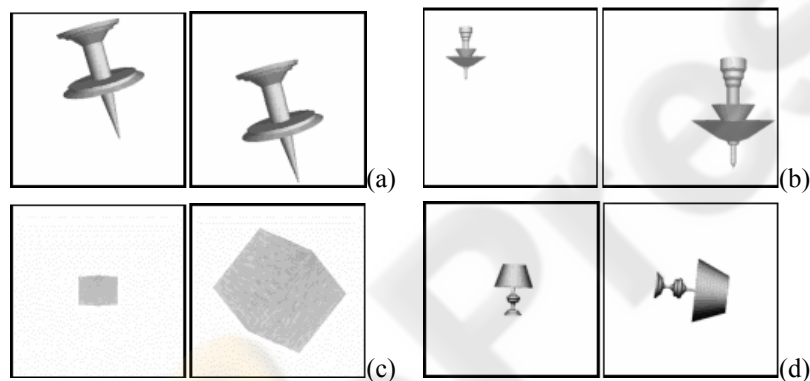


Fig. 3. (a) Thumbtack sequence frames 1 and 20. (b) Irregular form sequence frames 1 and 20. (c) Cube sequence frames 1 and 20. (d) Lamp sequence frames 1 and 20

4 Conclusions

In this paper, the LIAC model to spatio-temporally segment a moving object present in a sequence of images has been introduced. In first place, this method takes advantage of the inherent motion present in image sequences. This object segmentation method may be compared to background subtraction or frame difference algorithms in the way motion is detected. Then, a region growing technique is performed to define the moving object. In contrast to similar approaches no complex image pre-processing must be performed and no reference image must be offered to this model. The method facilitates any higher-level operation by taking advantage of the common charge value of parts of the moving object.

That is reason why it is so easy to introduce a simple but effective method for object tracking. To some extent, the line of research on tracking using interframe matching and affine transformations has been followed. Similarly to [9], the method depends on the assumption that the image structure constrains sufficiently reliable motion estimation. Firstly, the detection of an important parameter of an object in movement (its size) has been presented in this context. The algorithm is based on centroid tracking [10]. Lastly, comparing the results obtained in the previous stage towards a general graph for motion cases performs tracking. Compared to other approaches based on geometric properties, the method proposed assumes that the images in the sequences have a small transformation between them. Small changes over small regions are also assumed. In this approach, the number of tracking features is kept to a minimum. This permits to control one of the most important issues in visual systems: time.

Acknowledgements

This work is supported in part by the Spanish CICYT TIN2004-07661-C02-02 grant.

References

1. D. Hogg, "Model-based vision: A program to see a walking person", *Image and Vision Computing*, vol. 1, no. 1, pp. 5-20, 1983.
2. J.L. Barron, D.J. Fleet, S.S. Beauchemin, "Performance of optical flow techniques", *International Journal of Computer Vision*, vol. 12, no. 1, pp. 43-77, 1994.
3. R. Jain, W.N. Martin, J.K. Aggarwal, "Segmentation through the detection of changes due to motion", *Computer Graphics and Image Processing*, 11, pp. 13-34, 1970.
4. M.A. Fernández, J. Mira, "Permanence memory: A system for real time motion analysis in image sequences", in *IAPR Workshop on Machine Vision Applications, MVA'92*, 1992, pp. 249-252.
5. T.S. Huang, A.N. Netravali, "Motion and structure from feature correspondences: A review", *Proceedings of the IEEE*, 82, pp. 252-269, 1994.
6. R. Deriche, O.D. Faugeras, "Tracking line segments", *Image and Vision Computing*, vol. 8, no. 4, pp. 261-270, 1990.
7. A. Fernández-Caballero, Jose Mira, Ana E. Delgado, M.A. Fernández, "Lateral interaction in accumulative computation: A model for motion detection", *Neurocomputing*, 50C, 2003, pp. 341-364.
8. A. Fernández-Caballero, J. Mira, M.A. Fernández, A.E. Delgado, "On motion detection through a multi-layer neural network architecture", *Neural Networks*, 16 (2), 2003, pp. 205-222.
9. M. Gelgon, P. Bouthemy, "A region-level motion-based graph representation and labeling for tracking a spatial image partition", *Pattern Recognition*, 33 (4), 2000, pp. 725-740.
10. G. Liu, R. M. Haralick, "Using centroid covariance in target recognition," *Proceedings ICPR98*, 1998, pp. 1343-1346.